Hyperspectral characterization of freezing injury and its biochemical impacts in oilseed rape leaves

Chuanwen Wei[a,c], Jingfeng Huang[a,c,*], Xiuzhen Wang[d], George Alan Blackburn[e], Yao Zhang[a,b], Shusen Wang[f], Lamin R. Mansaray[a,c,g]

[a] Institute of Applied Remote Sensing and Information Technology, Zhejiang University, 310058 Hangzhou, China

[b] Key Laboratory of Environment Remediation and Ecological Health, Ministry of Education, College of Natural Resources and Environmental Science, Zhejiang University, 310058 Hangzhou, China

[c] Key Laboratory of Agricultural Remote Sensing and Information Systems, Zhejiang Province, China, Zhejiang University, 310058 Hangzhou, China

[d] Institute of Remote Sensing and Earth Sciences, Hangzhou Normal University, 311121 Hangzhou, China

[e] Lancaster Environment Centre, Lancaster University, Lancaster, UK

[f] Canada Centre for Remote Sensing, Natural Resources Canada, Ottawa, ON, Canada

[g] Department of Agro-meteorology and Geo-informatics, Magbosi Land, Water and Environment Research Centre (MLWERC), Sierra Leone Agricultural Research Institute, Tower Hill, Freetown, PMB 1313, Sierra Leone

[*] Corresponding author at: Institute of Applied Remote Sensing and Information Technology, Zhejiang University, 310058 Hangzhou, China. Tel.: +86 571 88982830.

E-mail addresses: weichuanwen@zju.edu.cn (Ch. Wei), hjf@zju.edu.cn (J. Huang).

Abstract:

Automatic detection and monitoring of freezing injury in crops is of vital importance for assessing plant physiological status and yield losses. This study

investigates the potential of hyperspectral techniques for detecting leaves at the stages of freezing and post-thawing injury, and for quantifying the impacts of freezing injury on leaf water and pigment contents. Four experiments were carried out to acquire hyperspectral reflectance and biochemical parameters for oilseed rape plants subjected to freezing treatment. Principal component analysis and support vector machines were applied to raw reflectance, first and second derivatives (SDR), and inverse logarithmic reflectance to differentiate freezing and the different stages of post-thawing from the normal leaf state. The impacts on biochemical retrieval using particular spectral domains were also assessed using a multivariate analysis. Results showed that SDR generated the highest classification accuracy (>95.6%) in the detection of post-thawed leaves. The optimal ratio vegetation index (RVI) generated the highest predictive accuracy for changes in leaf water content, with a cross validated coefficient of determination (R^2cv) of 0.85 and a cross validated root mean square error (RMSEcv) of 2.4161 mg/cm^2. Derivative spectral indices outperformed multivariate statistical methods for the estimation of changes in pigment contents. The highest accuracy was found between the optimal RVI and the change in carotenoids content (R^2_{CV}=0.70 and $RMSE_{CV}$=0.0015 mg/cm^2). The spectral domain 400-900 nm outperformed the full spectrum in the estimation of individual pigment contents, and hence this domain can be used to reduce redundancy and increase computational efficiency in future operational scenarios. Our findings indicate that hyperspectral remote sensing has considerable potential for characterizing freezing injury in oilseed rape, and this could form a basis for developing satellite remote sensing products for crop monitoring.

Keywords: hyperspectral reflectance; oilseed rape; freezing injury; detection; estimation; biochemical parameters

1 Introduction

Winter oilseed rape (*Brassica napus* L.) is an important oilseed crop in China. This crop is mainly cultivated in the Yangtze River basin. Because of the impact of cold spells, winter oilseed rape in this region is frequently subjected to freezing injury, which can lead to a significant decrease in yield and product quality (She et al., 2015; Zhang et al., 2008). Similar negative impacts of freezing are experienced by many different crop types globally (Cromey et al., 1998; Lardon & Triboi-Blondel, 1995; Staggenborg & Vanderlip 1996). Freezing injury is a common weather-induced agricultural hazard and refers to plants suffering from damage when temperatures drop below 0°C. When leaves are exposed to freezing temperatures, ice crystals are formed between cells. Cellular dehydration can then occur because of the difference in water potential between the inside and the outside of the cell, which draws cytoplasmic water from the cell to the growing mass of extracellular ice. With the decrease in temperature, more water moves from the cytoplasm to intercellular spaces. Permanent freezing injury is caused when dehydration extends beyond the tolerance of the plant and/or ice produces mechanical pressure.

Traditionally, monitoring of freezing injury relies on visual surveys by technicians in the field. This approach is dependent on having staff with sufficient expertise. It is time consuming and labor-intensive. Thus, a more effective alternative approach is required for detecting freezing injury in vegetation. Hyperspectral remote sensing has been widely used as a nondestructive technique to monitor various biotic and abiotic stress factors

across different spatial scales (Galvao et al., 2011; Liu et al., 2002; Penuelas et al., 1993; Sankaran et al., 2010; Strachan et al., 2002). As the process of freezing injury tends to be fast (often within a few hours), it means that if hyperspectral remotely-sensed data are to be of value in monitoring the process, they need to be acquired at a high temporal resolution. However, currently available optical satellite data lack the spectral and temporal resolution required for monitoring freezing injury in real time. Several satellite missions have been planned to generate suitable data. These include the Geostationary Coastal and Air Pollution Events (GEO-CAPE) mission from the USA (Board, 2007), the Geostationary Environment Monitoring Spectrometer (GEMS) mission from Korea (Bak et al., 2013), and the Sentinel-4 mission from Europe (Berger et al., 2012), which will provide appropriate datasets multiple times per day. In this study, spectroradiometer data were acquired in a laboratory setting at the leaf scale to demonstrate the capabilities for monitoring freezing injury using hyperspectral data, an approach that would provide a basis for airborne and space-borne monitoring in future when remote sensing data of higher spatial, spectral and temporal resolutions become available.

At the leaf scale, the spectral reflectance characteristics across the visible (400-750 nm), near-infrared (750-1300 nm) and shortwave-infrared (1300-2500 nm) ranges are primarily determined by variations in photosynthetic pigment content, leaf structure and water content (Knipling, 1970; Richardson et al., 2002; Slaton et al., 2001) which can be strongly impacted by freezing injury (Gausman et al., 1984; Wang et al., 2016; Wang et al., 2012). Many studies have been carried out on the potential of using hyperspectral techniques in evaluating the quality and safety attributes of food products (e.g. meat and

edible fungi) subjected to freeze damage (Gowen et al., 2009; Thyholt & Isaksson, 1997). Gowen et al. (2009) integrated principal components analysis and linear discriminant analysis to differentiate between undamaged and freeze-damaged mushrooms using hyperspectral imaging. Their results indicated that freeze-damaged mushrooms could be classified with high accuracy (>95%) after only 45 minutes of thawing. Other studies have used hyperspectral data to estimate the changes in biophysical or biochemical parameters after freezing injury. Nicotra et al. (2003) examined the impact of freezing stress on the distribution of photosynthetic pigments in *Eucalyptus pauciflora* leaves using a CASI high-resolution hyperspectral imaging system. Their results demonstrated a considerable spatial variation of chlorophyll content over the surface of the lamina, with marked decreases in chlorophyll content approaching the margins and tips of the leaves. However, changes in the hyperspectral characteristics of crops such as oilseed rape during the freezing injury process are yet to be investigated, and the potential of using hyperspectral techniques to identify leaf status and monitor biochemical changes remains unknown.

A variety of different analytical techniques have been used to automatically detect and classify plant stress from remotely sensed data. Amongst these techniques, support vector machines (SVMs) are promising machine learning methods which are suitable for remote sensing applications due to their ability to generalize well even with limited training samples (Mantero et al., 2005). SVMs have already been used in land cover classification (Gao et al., 2015; Hong et al., 2015; Zhang et al., 2015), quantifying vegetation stress (Adjorlolo et al., 2015; Behmann et al., 2014) and land cover change

111 detection (Hichri et al., 2013; Hussain et al., 2013; Nemmour & Chibani, 2006).
112 Furthermore, SVMs have been used to estimate plant biophysical and biochemical
113 parameters such as LAI, biomass, pigments and nitrogen contents (Gleason & Im, 2012;
114 Verrelst et al., 2012; Yang et al., 2011; Zhai et al., 2013). Hence, SVMs hold promise as a
115 method for characterizing freezing injury in plants using hyperspectral data.

116 Multi-collinearity is a common problem within hyperspectral data. It results from a
117 large number of highly correlated wave bands. Some techniques have been proposed to
118 reduce the redundancy of hyperspectral data for vegetation applications. Principal
119 component regression (PCR) and partial least square regression (PLSR) can be employed
120 to solve multi-collinearity problems. Many studies have used these techniques to
121 construct predictive relationships between spectral data and vegetation parameters
122 (Adjorlolo et al., 2015; Gonzalez-Fernandez et al., 2015). In order to reduce redundancy
123 in spectral data, some studies have made a comparison between the full spectrum and
124 specific spectral domains (ranges) for estimating vegetation parameters from remotely
125 sensed hyperspectral data using multivariate models (Gonzalez-Fernandez et al., 2015;
126 Darvishzadeh et al., 2008; Huang & Blackburn, 2011). The results indicate that predictive
127 models based on specific spectral domains are superior to models based on the full
128 spectrum. Hence, there is considerable potential for the use of spectral indices,
129 multivariate regression techniques and optimized spectral domains for assessing freezing
130 injury in vegetation using hyperspectral data, and this warrants further investigation.

131 The overall aim of this study is to determine the applicability of leaf spectral
132 reflectance data for detecting the freezing and post-thawing states of oilseed rape and

quantifying the biochemical impacts of freezing. The objectives are to (1) characterize the spectral reflectance of oilseed rape leaves during freezing and post-thawing; (2) identify appropriate analytical techniques that can be applied to reflectance spectra to differentiate between normal leaves and leaves at freezing and different stages of post-thawing; (3) establish predictive models based on leaf spectral reflectance measurements for quantifying the changes in leaf water content (ΔLWC), chlorophyll a (ΔChla), chlorophyll b (ΔChlb), and carotenoids (ΔCars) induced by freezing injury.

2 Materials and methods

2.1 Plant culture and experimental design

The experiments were conducted at the Campus Experimental Station of Zhejiang University. The seeds were a local commercial variety of oilseed rape (Zheyou No.50). The soil used for this study was paddy soil. The seeds were sown in black plastic pots (18 cm diameter ×16 cm height) on October 13, 2013 and October 20, 2014, and were located outdoors. The seedlings were thinned to two plants per pot at the 3-leaf stage. Plants were watered as necessary and fertilizer was applied according to local agronomic practices. Treatments were carried out at the 8 leaf-stage during the 2013-2014 growing season, while treatments were carried out at the initial stage of budding during the 2014-2015 growing season. The air temperature profile during the growing period is given in Fig. 1.

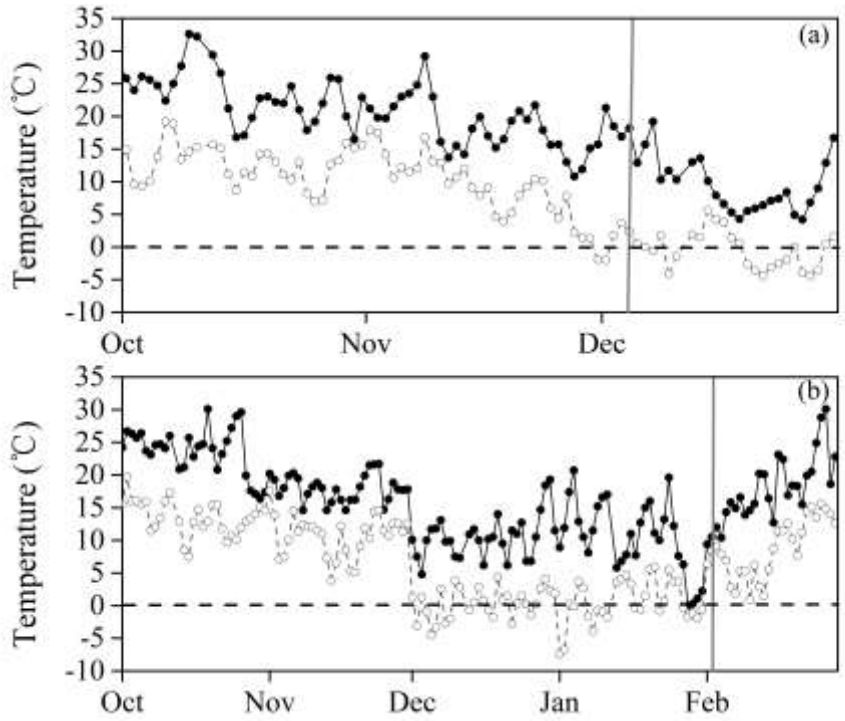

Fig. 1. Minimum and maximum daily temperatures in Hangzhou, China; (a) between October 2013 and December 2013, and (b) between October 2014 and February 2015. The treatment dates are indicated by gray vertical bars. Closed and open circles represent maximum and minimum temperature, respectively.

Each pot containing two plants was transferred to an Aucma freezer (390L in Volume). The freezing of plants was executed under conditions of darkness. Air temperature decreased from laboratory temperature to the lowest temperature range of -10~-12 ℃. As the formation of rime on the leaves could affect hyperspectral measurements in various ways desiccants were applied to reduce the relative humidity within the freezer during the freezing treatments. Before each measurement, we ensured that there was no rime/frost on the observed leaf surfaces based on visual observation. Leaf temperature was monitored at one second intervals by a digital temperature sensor with a precision of ± 0.5℃（-10℃～+85℃）. The temperature sensor was connected to

a computer on which a 8-channel temperature data acquisition software was installed to log data. The time course of leaf temperature during a typical freezing treatment is shown in Fig. 2. After treatment, the plants were transferred to a light incubator to thaw at 22℃ day/18℃ night temperatures with an 11 hour photoperiod (7 am–6 am) and light intensity of 8000 LX.

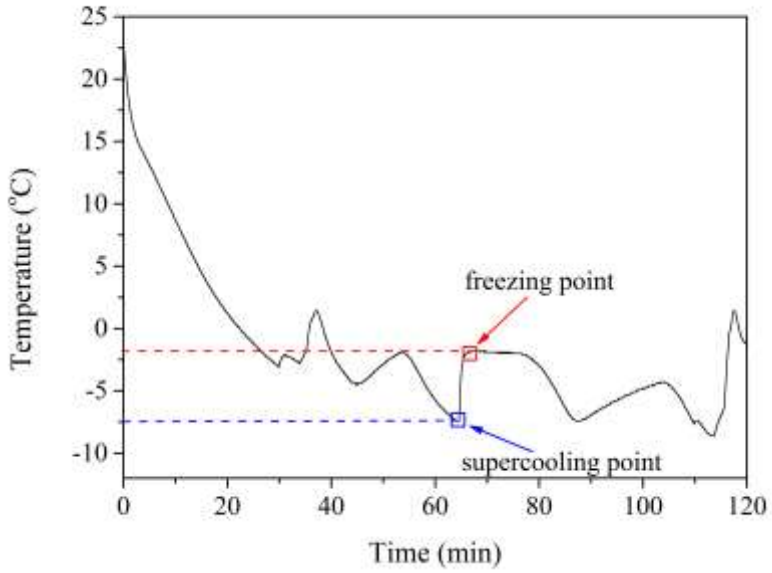

Fig. 2. Changes of leaf temperature during freezing treatment.

Experiment 1: Changes in cell structure and water content due to freezing.

To determine the effect of freezing on leaf cell structure and water content, 29 pots (samples) were used in this study, with 3 pots treated on each day in the morning, afternoon and night, respectively. A small leaf strip was cut for creating an image of the cross-section in the symmetric right side of the normal leaf. At the same time, three discs were cut from the same side of the leaf with a punch to obtain a measurement of water content. The same procedures were performed on the left side of the leaf 1 hour after the onset of freezing which was detected as a rapid increase in leaf temperature (Brown et al.,

1974; Burke et al., 1976).

Experiment 2: Spectral changes over different lengths of freezing.

One leaf sample from a plant was first used to acquire reflectance at the normal state at 8 am. Following the onset of freezing, reflectance of the leaf was measured repeatedly after 10 min, 30 min, 1 hr and then at 1 hr intervals for 10 hrs. Five different plants were measured in this way over a period of 5 days with 1 plant per day.

Experiment 3: Spectral changes during the process of post-thawing.

Spectral reflectance was measured initially on a leaf sample in the normal state at 8 pm prior to freezing treatment. When the leaf had been frozen for 1hr, reflectance was measured again. After subjecting the plant to eleven hours of freezing treatment, thawing was initiated and the spectral reflectance of the leaf was measured repeatedly after 2, 4, 6, 8, 27, 30, 33, 51, 54 and 57 hrs. Concurrently with each spectral reflectance measurement, a SPAD chlorophyll meter was used to obtain a relative measure of chlorophyll content. In addition, the SPAD values of the leaf in supercooled and frozen states were also measured. The measurement of 26 samples, with 4 pots per day, required a total of 8 days.

Experiment 4: Changes in biochemical parameters following thawing.

The spectral reflectance of a leaf in the normal state was measured initially on the left side of the midrib at 8 pm. At the same time, water and pigment contents were measured on the symmetric right side of the leaf by destructive sampling. The plant was then put into the freezer and treated for eleven hours. After post-thawing for two hours in the light incubator, spectral reflectance, water and pigment contents were measured on the

left side of the midrib of the leaf. The same procedures were implemented for other leaf samples after post-thawing for 2-58 hrs with an increment of two hours until the leaf became air-dry in the incubator. Three leaves were measured at each time. We expressed the variations in the biochemical parameters as the difference (Δ) between pre and post treatment, which can effectively eliminate the effect of different leaf samples and time variation. The measurement of 29 plants, with 6 pots per day, required a total of 6 days.

2.2 Measurement of leaf reflectance

Leaf reflectance was measured using a FieldSpec 3 spectroradiometer (Analytical Spectral Devices, Boulder, USA) for Experiments 2-4 in 2015. This instrument has a spectral range from 350 to 2500 nm, with a 1.4 nm sampling interval between 350 and 1000 nm and 2 nm sampling interval between 1000 and 2500 nm. The spectral resolution of the FieldSpec 3 is 3 nm for the region 350-1000 nm and 8 nm for the region 1000-2500 nm. The fiber-optic probe of the spectroradiometer was routed into the freezer so that leaf reflectance measurements could be performed while plants were undergoing treatment, thereby avoiding any disruption to treatment caused by the removal of plants from the freezer for reflectance measurements. The probe was positioned to look down vertically from a height of 3 cm above the leaf, giving a field of view of 1.3 cm^2 at the leaf surface. When measuring leaf reflectance at a particular state, the irradiance incident upon each leaf was first measured by obtaining a radiance spectrum of a white Spectralon panel (Labsphere, North Sutton). The leaf to be measured was then fixed on a lifting platform covered in black cardboard with a round hole of 3 cm in diameter and the leaf was kept at the same height as the white panel

surface by adjusting the platform. This setup ensured that the same area of each leaf was repeatedly measured. In order to minimize the impact of background reflectance, a black cover of 2% reflectance was used as the background beneath the leaf. The light source was a 50W quartz halogen lamp which was turned on for the short duration of the reflectance measurements and had no discernable effect on leaf temperature. The angle between the leaf surface and the incident beam was 45°. The interior of the freezer was coated with black material to avoid scattered ambient light. The % reflectance of the leaf was calculated by dividing the leaf radiance by that of the white panel, applying a correction factor for the panel reflectance properties. Ten spectra were recorded and then averaged to represent the leaf reflectance.

2.3 Measurement of biochemical variables

2.3.1 Chlorophyll and carotenoid contents

In order to acquire the time-series information on chlorophyll content during freezing injury, we employed a nondestructive approach using a SPAD (Minolta, Inc.) to measure the relative chlorophyll content. SPAD readings were taken six times at the leaf margin and their average was considered as the SPAD value of the leaf.

For estimating the absolute changes in pigment content, for each leaf sample, three leaf discs (totaling 1.69 cm^2) were obtained using a hole punch, which were then cut into thin strips using scissors. These strips were extracted with 80% acetone in the dark till turning white. The absorbance of the supernatant was measured at 470, 646.8 and 663.2 nm with a spectrophotometer (Model UV2550, Shimadzu Corporation, Tokyo, Japan). The contents of chlorophyll a, chlorophyll b and carotenoids were determined using the

formulae of Lichtenthaler (1987).

2.3.2 Leaf water content

For each leaf sample, three leaf discs were obtained for the measurement of water content. The fresh weight was measured, after which the discs were dried to a constant mass in an oven at a temperature of 70°C. The leaf water content (LWC) was calculated as follows:

$$LWC= (FM- DM)/A \quad (1)$$

where, FM is the leaf fresh mass (g), DM is the oven dry leaf mass (g), and A is the area of three leaf discs (cm^2).

2.4 Leaf histology

To examine the cellular structure of normal and frozen leaves, some small strips (approximately 1 mm × 7 mm) were cut from the leaf samples. The specimens were fixed immediately with 3% glutaraldehyde in a 0.015 mol/L phosphate buffer (pH6.9) then air in the strips was pumped out using a syringe until the sections sank to the bottom of a Penicillin bottle. The specimens were put in the refrigerator for more than four hours at 4℃. After that, the strips were washed three times in phosphate buffer (0.1M, pH7.0) for 15 min at each time. The strips were fixed again using 1% OsO_4 in phosphate buffer (0.1M, pH7.0) for 1-2 hrs, and then washed three times in the same way. The dehydration process was conducted using a graded ethanol series (30%, 50%, 70%, 80%, 90%, 95%, 100%) for 15-20 min at each step, and the strips were embedded with Spurr resin following Li and Zhang (2003). Sections of 3-4 μm thickness were sliced using the glass blade on LEICA EM UC7 Ultratome and stained with 0.5% toluidine blue in 0.1% sodium

carbonate buffer (pH9.0) for light microscopy, and uranyl acetate and alkaline lead citrate for transmission electron microscopy. Images of the sections were taken using a light microscope (400 × magnification) and a digital camera.

2.5 Data analysis

From all leaf reflectance spectra collected, the wavelength range between 400 nm and 2400 nm was retained for analysis due to high noise levels at both ends of the spectra. The original spectra were then smoothed using a Savitzky–Golay filter with 15 sample points and a second order polynomial (Savitzky & Golay, 1964). The atmospheric water absorption wavebands located at 1350-1480 nm and 1780-1990 nm were also removed from the spectra before further analysis.

2.5.1 Spectral data manipulation

To quantify changes in spectral shape and magnitude with time, we computed the θ and D indices as described by (Price, 1994):

$$\theta = \arccos\left(\frac{\sum_{i=1}^{N} S_r * S_s(\lambda_i)}{\left[\sum_{i=1}^{N} S_r^2\right]^{1/2} * \left[\sum_{i=1}^{N} S_s^2(\lambda_i)\right]^{1/2}}\right) \quad (2)$$

$$D = sqrt\left(\frac{\sum_{i=1}^{N} \left(S_r - S_s(\lambda_i)\right)^2}{N}\right) \quad (3)$$

where, λi is the wavelength at band i, N is the number of bands, Ss is the sample spectrum, and Sr is the reference spectrum which is a constant set at 1, representing the maximum of reflectivity. The θ value represents the angle between the reference and the

sample spectrum, calculated using a vector dot product. The D value calculates the root mean square difference between the sample spectrum reflectance amplitude and the reference spectrum amplitude.

The θ and D indices were calculated for the following wavelength regions: 400 to 2400 nm (full spectrum: VIS, NIR, and SWIR), 400 to 750 nm (visible), 751 to 1000 nm (near infrared 1), 1001 to 1350 nm (near infrared 2), 1351 to 1800 (short-wave infrared 1), and 1801 to 2400 nm (short-wave infrared 2). The near infrared and the short-wave infrared were divided according to the wavelength limits of individual detectors within the FieldSpec 3 instrument.

2.5.2 Techniques for classification

In addition to using raw spectral reflectance (Raw), the first derivative (FDR), second derivative (SDR) and the inverse logarithm (Log (1/Raw)) of raw reflectance were calculated for discriminating normal leaves from freezing and post-thawing leaves. Derivative techniques can eliminate background signal and separate closely related absorption features (Demetriadesshah et al., 1990). Log (1/Raw) can enhance differences in spectral features in the visible range and reduce the effect of multiplicative factors (Clark & Roush, 1984). We then identified reflectance data that had significant differences between leaves in the normal and freezing 1 hour states and those at different phases of post-thawing by performing mixed effect model analysis with multi-means comparison for all wavebands in the Raw spectra and the various spectral transformations. The nlme package in R software was used to establish the linear mixed effect model and multiple comparisons were conducted using the lsmeans package.

Wavebands with a p-value <0.05 were selected as initial candidates. In the final procedure, principal components were used as inputs variables in the SVMs (see section 2.5.3) and the number of principal components used was determined according to the criteria of cumulative contribution >90%.

2.5.3 Techniques for retrieval

For the retrieval of ΔLWC, five different spectral domains were tested (Table 1). The first was the full spectrum with the atmospheric water vapor absorption wavelengths removed, as these wavelengths cannot be used in space-borne remote sensing. The other four regions were selected based on the description of Jensen (2006), where it was found that the shortwave infrared intervals appear to be more sensitive to changes in plant moisture content than the visible or near infrared portions of the spectrum. For the retrieval of ΔChla, ΔChlb and ΔCars, two domains were tested (Table 1). The first domain was selected by removing atmospheric water absorption wavelengths, while the other was based on the results of Huang & Blackburn (2011) which showed that the spectral wavelength domain 400-900 nm is optimal for quantifying leaf chlorophyll concentration. These spectral domains have been tested and selected in the aforementioned articles and we intended to verify their utility in our study.

Table 1. Spectral domains tested for biochemical parameters estimation.

Parameter	Spectral domain
ΔLWC	400-2400 nm, 400-750 nm 751-1349 nm, 1481-1779 nm 1991-2400 nm

ΔChla, ΔChlb, ΔCars	400-2400 nm, 400-900 nm

We used two methods to estimate the changes in leaf traits based on leaf spectral properties. The first approach correlated spectral vegetation indices (VIs) and measured biophysical parameters. This method has an advantage of fast processing speed. We chose two of the most widely used vegetation indices: ratio index (Jordan, 1969) and normalized difference vegetation index (Rouse et al., 1974) for the estimation of biophysical parameters. To determine the optimal narrow band index, all possible combinations of two bands were calculated and the combination that produced the highest coefficient of determination (R^2) with leaf biophysical parameters was identified. The first derivative reflectance was used to optimize the VIs for ΔLWC and Δpigment content estimation as it exhibited the stronger relationship with the change in biochemical parameters than raw reflectance.

In the second approach, the statistical methods PCR, PLSR and SVMs, which exploit information from the full leaf spectrum, were examined. PCR reduces data redundancy by transforming a set of highly correlated variables into a new set of uncorrelated principal components variables (Ye et al., 2008). Both the PCR and PLSR methods have similar structures and are able to avoid the multi-collinearity problem. Whereas PCR performs the decomposition on the spectral data alone, PLSR uses the response variable information during the decomposition process and performs the decomposition on both the spectral data and the response variable simultaneously (Inoue et al., 2012). For PCR, the number of PCs was chosen based on two methods (Mirzaie et al., 2014): (1) percent variance explained in the spectral data and (2) cross-validated

RMSE (root mean square error). For PLSR, a leave-one-out cross-validation was employed to determine the number of factors by setting the condition that adding an extra factor must reduce the cross-validated RMSE by >2% (Kooistra et al., 2004). The PCR and PLSR analyses were performed using the pls (Mevik & Wehrens, 2007) package developed in R software (version 3.3.0; Team 2014).

SVMs are a supervised machine learning method. The basic theory behind SVMs is to seek the optimal separating hyperplane with the maximum margin, which is the goal of statistical learning theory. In contrast to parametric regression methods in which explicit relationships between spectral observations and biophysical variables are obtained, SVMs provide excellent generalization capabilities, are fast, robust to high input space dimensions and low numbers of samples. SVMs provide sparse solutions where only the most relevant samples of the training data are weighted, resulting in low computational cost and memory requirements. We performed a C-SVC (support vector classification) by minimizing the following objective function (Boser, 1992; Cortes & Vapnik, 1995):

$$\min_{\omega,b,\varepsilon} \quad \frac{1}{2}\boldsymbol{\omega}^{T}\boldsymbol{\omega} + C\sum_{i=1}^{n}\xi_{i} \tag{4}$$

$$\text{subject to} \quad \begin{aligned} & y_{i}\left(\boldsymbol{\omega}^{T}\phi\left(X_{i}\right) + b\right) \geq 1 - \xi_{i,} \\ & \xi_{i} \geq 0 \end{aligned} \tag{5}$$

where, ω and b represent the normal vector and bias of the hyperplane, respectively. x_i ϵR^n is an m-dimensional feature vector, y_i ϵ[-1,1] is the class label, i=1,…,n. C >0 is penalty value and ξ_i ϵR^n is the slack variable that indicates the distance the sample is from the hyperplane passing through the support vectors of the class to which the sample

belongs, and $\Phi(x_i)$ is the mapping function. In addition, we performed an ε-SVR (support vector regression) for inversion applications, which minimizes the following error function (Vapnik, 1998):

$$\min_{\omega,b,\xi,\xi^*} \quad \frac{1}{2}\omega^T\omega + C\sum_{i=1}^{n}\xi_i + C\sum_{i=1}^{n}\xi_i^* \tag{6}$$

$$\text{subject to} \quad \omega^T\phi(X_i) + b - Z_i \le \varepsilon + \xi_i, \tag{7}$$

$$Z_i - \omega^T\phi(X_i) - b \le \varepsilon + \xi_i^*,$$

$$\xi_i, \xi_i^* \ge 0, i = 1, \ldots, n.$$

where, $Z_i \in R^1$ is the target output and ε is the insensitive loss function that controls the approximation error. Given the nonlinear problems, we used the radial basis kernel function (RBF) to map the feature vectors into a high dimensional space. The RBF has been shown to be particularly effective in remote sensing applications (Foody & Mathur, 2004) and is defined as:

$$K(X_i, X_j) = \exp\left(-\gamma\left\|X_i - X_j\right\|^2\right), \gamma > 0 \tag{8}$$

where, γ is a parameter that controls the width of the kernel and x_j is the unknown feature vector. The accuracy of SVMs is dependent on the magnitude of the parameters C and γ. The latter is inversely proportional to the Gaussian kernel width which determines the computing window of the RBF kernel matrix, while the former controls the penalty associated with training samples which lie on the wrong side of the decision boundary. We optimized these two parameters with a five cross-validated grid search method to avoid over-fitting. The range of C and γ were both [-10, 10] and the steps used were 0.5 for both SVC and SVR applications. The LIBSVM 3.20 toolbox (Chang &

389 Lin, 2011) was used for the SVMs analyses in the MATLAB environment.

390 **2.5.4 Accuracy evaluation and model performance**

391 Overall accuracy and Kappa coefficient which are the most commonly used indices
392 for accuracy assessment of remote sensing data (Foody, 2002) were chosen to evaluate the
393 accuracy of SVMs for identifying the status of leaves during freezing injury.
394 Approximately, 75% of the samples were used to train the SVMs and the 25% remaining
395 was used for validation. The whole data set was randomly divided 100 times for repeated
396 accuracy assessments and the average values for the indices were used for accuracy
397 evaluation. To evaluate and compare the predictive models for leaf water and pigments,
398 R^2, RMSE and relative error (RRMSE that is RMSE divided by the sample mean) were
399 used as indicators for this study. The method used for model validation was the
400 leave-one-out cross-validation.

401 **3 Results and discussions**

402 **3.1 Biochemical analysis**

403 A paired-sample t-test showed that there was no significant difference in water
404 content between normal and frozen leaves ($p=0.648$, $\alpha=0.05$). Fig. 3 shows the changes
405 in SPAD values for oilseed rape leaves at the stages of supercooling, freezing and
406 post-thawing. As indicated in this figure, the paired-sample t-test also confirmed that
407 there was no significant difference in relative chlorophyll content between normal and
408 frozen leaves ($p=0.056$, $\alpha=0.05$). However, there was a significant decline in relative
409 chlorophyll content after 2 hours of post-thawing. As post-thawing progressed, the
410 SPAD values became more variable across the samples tested. This was due to the wide

411 uncertainty in SPAD measurements.

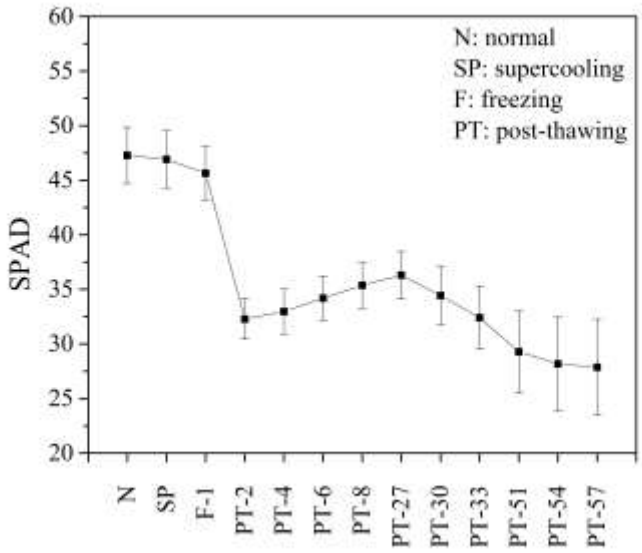

412

413 Fig. 3. Average SPAD values of oilseed rape leaves at the normal, supercooling, 1hr of freezing and at

414 different hours of post-thawing. The bars represent ± 95% confidence interval (CI) (n=26).

415 **3.2 Structural changes of mesophyll cells**

416 Cross-sections of normal and freeze-damaged oilseed rape leaves are presented in

417 Fig. 4. In the normal leaf, the mesophyll cells are turgid and the chloroplasts are arranged

418 along the cell walls (Fig. 4a). A more detailed electron micrograph is shown in Fig. 4c.

419 When plant tissues are subjected to freezing temperatures, ice commonly forms in the

420 intercellular spaces due to the higher freezing point than that in the cytoplasm (Croser et

421 al., 2003; Xin & Browse, 2000). Because of ice formation, the water potential outside the

422 cell drops, which can lead to cellular dehydration and therefore, cell collapse (Guy, 1990).

423 This effect is demonstrated in Fig. 4b for the freeze-damaged leaf, where cell walls have

424 become irregular and the proportion of intercellular air-spaces has increased due to cell

425 contraction. The internal structures of cells such as organelles and plasma membrane have

426 been severely disrupted (Fig. 4d).

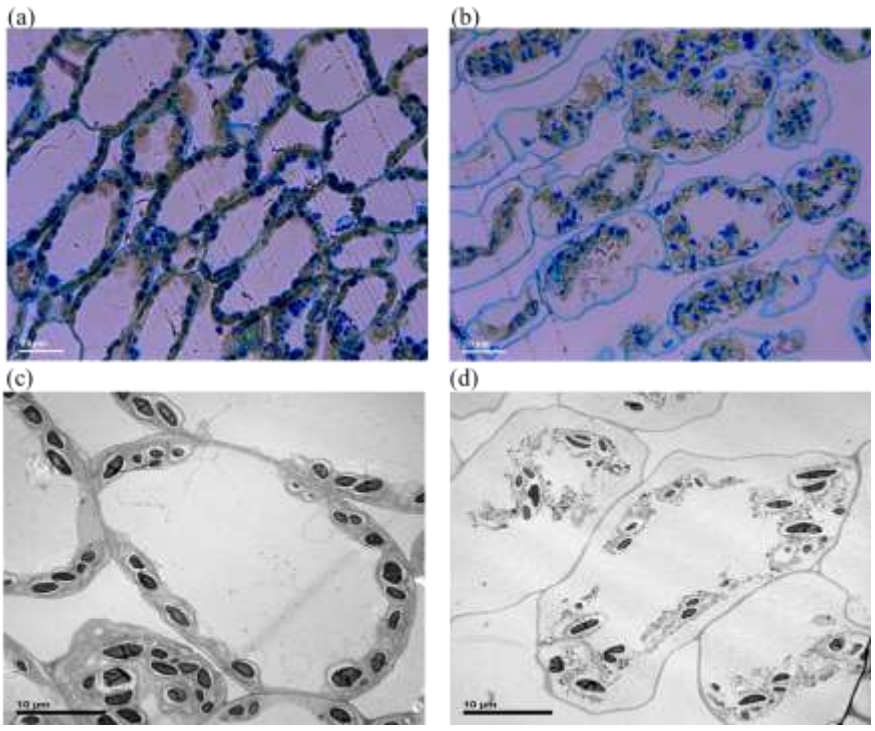

Fig. 4. Light microscopic images (a, b) and transmission electron micrographs (c, d) showing transverse section of normal (a, c) and freeze-damaged (b, d) oilseed rape leaves.

3.3 Leaf spectral reflectance

Changes in the spectral reflectance of leaves during freezing are depicted in Fig. 5a. It can be observed that reflectance decreases gradually with the duration of freezing. The water absorption features shifted gradually to longer wavelengths until all the water inside the leaf became frozen. D and θ, calculated from different wavelength intervals revealed the temporal trends of local spectral domains (Fig. 6 (a-f)). D gradually increased over time for all wavelength domains until the values remained relatively constant. θ values were generally constant for most of the spectral range except SWIR1 which increased at first then remained constant after 30 min of freezing. Increasing D values represents a decrease in reflectance magnitude, while decreasing θ represents a flattening of the spectral shape.

441 Because the SPAD values and water content displayed no significant changes
442 between normal and frozen leaves (see section 3.1), we surmised that the changes in
443 reflectance were mainly attributable to modifications in cellular structure. As seen from
444 the microscopy (Fig. 4), freezing injury was manifested as a disruption of cell wall
445 configuration, increase in intercellular spaces and disintegration of cell contents which are
446 likely to result in alterations of the refractive index within the leaf and a decrease in
447 scattering of incident light. These changes contributed to the decrease of leaf reflectance
448 throughout the spectrum. Because the peaks in the absorption coefficient of ice are at
449 longer wavelengths than those of liquid water (Green et al., 2006), the positions of the
450 water absorption features in leaf reflectance spectra shift to longer wavelengths when leaf
451 water is transformed into ice upon freezing. In the case of the first strong water absorption
452 feature, the wavelength corresponding to the minimum reflectance moved from 1456 nm
453 to 1486 nm as leaves moved from the normal state to being frozen for 10 minutes. After
454 the leaves were frozen for an hour, the movement of the water absorption feature became
455 much smaller (<5 nm). As we can see from Fig. 5a, a spectral peak at about 750 nm
456 occurred on the near-infrared shoulder for the frozen leaves. This phenomenon is related
457 to chlorophyll fluorescence (Gamon & Surfus, 1999) which is induced by a sudden
458 conversion of plant tissues from dark-adapted to high light conditions within a few
459 seconds, which is an indicator of photosynthetic performance (Gamon et al., 1990). As
460 the control plants were not incubated in the dark before the reflectance measurements
461 this peak was not detectable for the controls.

462 Fig. 5b reveals the changes in the reflectance of oilseed rape leaves during

post-thawing. In contrast to the frozen leaves, the water absorption features in the spectra of post-thawed leaves returned to their initial wavelength positions, as in the normal leaf. Leaf reflectance for all spectral intervals at 2 hours of post-thawing decreased significantly relative to control leaves (Fig. 6 (g-l)). Reflectance in the visible region decreased at first, then remained constant, and rapidly increased after 30 hours of post-thawing. Reflectance generally decreased in the NIR1 region, whereas in the NIR2 region it increased with the duration of post-thawing. For both SWIR1 and SWIR2 domains, D and θ gradually decreased over time after 2 hours of post-thawing. At that stage of post-thawing, the water absorption bands at 970 nm, 1200 nm, 1450 nm and 1940 nm virtually disappeared and the dry matter absorption features became more prominent, such as those for lignin, cellulose, starch and protein at 1690 nm , 1900 nm, 2130 nm and 2300 nm (Curran, 1989). Such findings concur with Carter (1991), who demonstrated that a water deficit can alter cell structure and chemistry such that the leaf reflectance throughout the 400-2500 nm wavelength range can be affected.

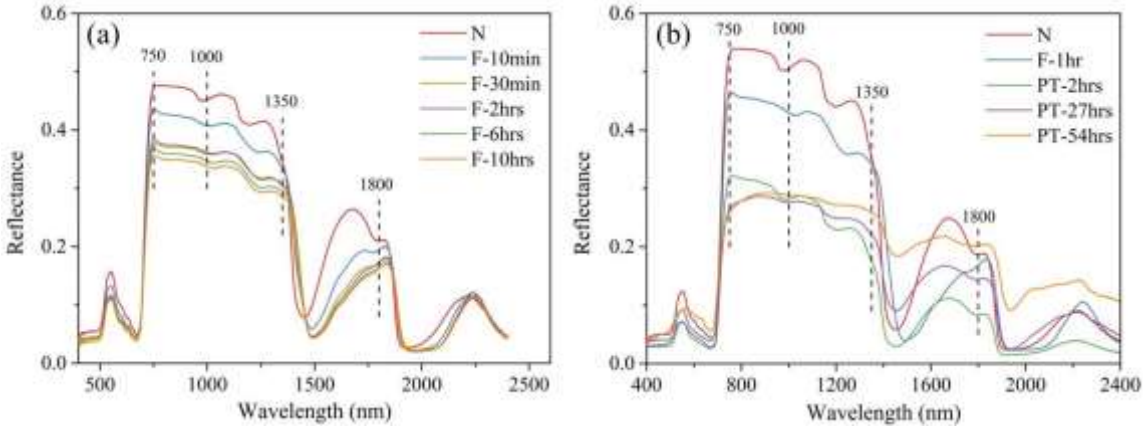

Fig.5. Response of leaf reflectance spectra at different phases of freezing injury: (a) changes in average reflectance with freezing; (b) changes in average reflectance with post-thawing. N, F and PT represent normal, freezing and post-thawing in the Legend. Wavelength regions are marked by

vertical dashed lines. The total sample sizes are 5 and 26, respectively.

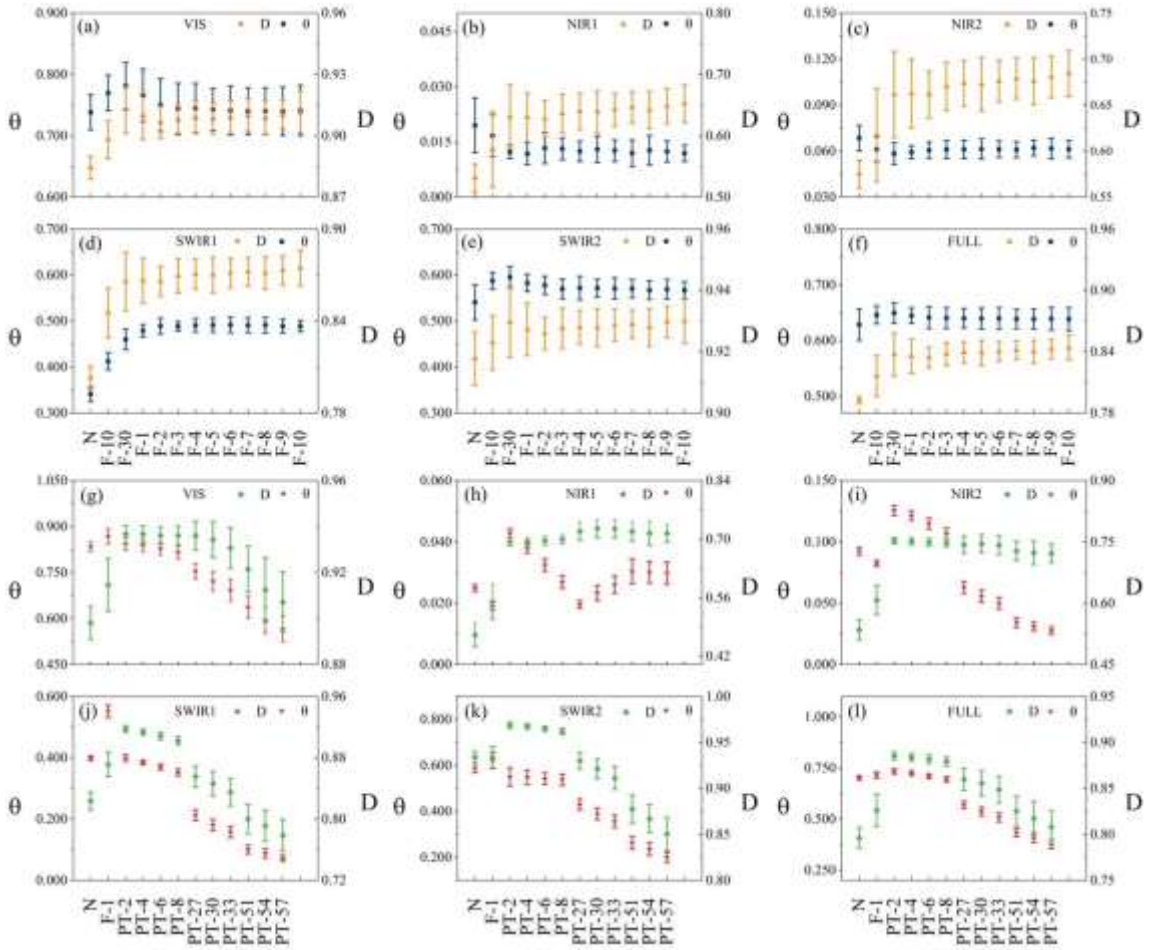

Fig. 6. Change in indices θ and D; (a-f) during freezing, and (g-l) post-thawing. N represents normal state, F-digit denotes the duration of freezing, PT-digit means the time of post-thawing. Bars represent 95% confidence interval.

3.4 Identification of freezing and the different stages of post-thawing

The identification of leaves frozen for 1hr was effective with an overall accuracy >97.0% for various spectral transformations while the raw reflectance had relatively lower classification accuracy with an overall accuracy of 72.8% (Table 2). These results indicate that the derivative and logarithmic transformations of spectral reflectance were helpful for improving the identification of leaf states during freezing.

Although freezing changes water mobility in plant tissues and potentially also pigment content and composition, these are not necessarily lasting effects and some plants could possibly recover. In order to determine whether freezing injury continues, we need to identify further the different stages of post-thawing.

Table 2 shows the accuracy with which it is possible to discriminate between normal leaves and leaves that have undergone different durations of post-thawing. The lowest overall classification accuracy for all post-thawing durations is 93.0% based on raw reflectance. These high levels of classification accuracy are due to the fact that the spectral reflectance is significantly different between normal oilseed leaves and those at all stages of post-thawing (see Fig. 5b). In this study, leaves measured in the 2014-2015 growing season all became dry and yellow after 3 days of post-thawing. This is attributable to the long duration of freezing treatment (11 hours) and the rapid decrease and subsequent increase in temperature. The heavy freezing injury resulted in large variations of the raw reflectance during post-thawing, thus the classification accuracy was high when using raw reflectance.

However, SDR spectra were most effective for discriminating post-thawing leaves with an overall accuracy >95.6%. The overall accuracy based on SDR first reached 100% after 33 hrs of post-thawing relative to the other two spectral transformations. The reason for the differences among different transformed spectra types may be that the SDR can better distinguish the similar original spectra by separating the local region with different curvature into several groups (Tsai & Philpot, 1998).

514 Table 2. Classification results for the discrimination of normal leaves from leaves at different stages
515 of post-thawing based on raw reflectance and its spectral transformations. OA and KC are overall
516 accuracy and kappa coefficient, respectively. F-digit denotes the duration of freezing, PT-digit means
517 the time of post-thawing.

State (hour)	F-1	PT-2	PT-4	PT-6	PT-8	PT-27	PT-30	PT-33	PT-51	PT-54	PT-57
Raw_OA(%)	72.8	95.0	95.6	97.0	95.6	94.9	95.9	96.1	94.6	93.0	97.9
Raw_KC	0.46	0.90	0.91	0.94	0.91	0.90	0.92	0.92	0.89	0.86	0.96
FDR_OA(%)	98.1	95.3	96.1	96.4	95.9	97.9	98.1	97.9	98.3	98.3	99.5
FDR_KC	0.96	0.91	0.92	0.93	0.92	0.96	0.96	0.96	0.97	0.97	0.99
SDR_OA(%)	99.6	96.2	95.6	97.9	98.4	98.0	99.0	100.0	100.0	100.0	100.0
SDR_KC	0.99	0.92	0.91	0.96	0.97	0.96	0.98	1.00	1.00	1.00	1.00
Log(1/Raw)_OA(%)	97.0	92.7	95.5	96.2	96.1	96.3	97.1	97.9	100.0	100.0	100.0
Log(1/Raw)_KC	0.94	0.85	0.91	0.92	0.92	0.93	0.94	0.96	1.00	1.00	1.00

518 **3.5. Monitoring freezing injury based on the retrieval of leaf biochemical**
519 **parameters from reflectance spectra**

520 **3.5.1 Quantification of biochemicals using hyperspectral vegetation indices**

521 The optimal band combinations and their R^2 values are described in Table 3. Using
522 the 1314 nm and 1642 nm bands, RVI (R^2=0.87) had a stronger linear relationship with
523 ΔLWC than NDVI (0.81) using bands at 1135 and 1697 nm. Similarly, RVI had higher
524 R^2 values (0.68, 0.57, 0.73) than NDVI (0.64, 0.56, 0.65) for ΔChla, ΔChlb, ΔCars,
525 respectively. In previous studies the techniques used here has been applied to find the
526 optimal combination of wavebands using various types of spectral indices for estimating

leaf Chla, Chlb (Yu et al., 2014) and water content (Yi et al., 2013), and canopy biomass and LAI (Thenkabail et al., 2000) from a number of species. This study confirms that the method can provide a fast overview of thousands of wavelength combinations and make possible the detection of wavelengths of interest for further analysis.

Linear regression models were constructed between the optimal spectral indices and biochemical parameters. The optimal RVI had the highest accuracy in predicting ΔLWC with values of 0.85 for R^2_{CV} and 2.4161 for $RMSE_{CV}$. Ceccato et al. (2002) demonstrated that the SWIR region is sensitive to equivalent water thickness (EWT) but cannot be used alone to retrieve EWT because two other leaf parameters (internal structure and dry matter) also influence leaf reflectance in the SWIR. A combination of SWIR and NIR (only influenced by these two parameters) is necessary to retrieve EWT at leaf level. In our study, although the strong water absorption bands were removed, the selected wavelengths were still located in the NIR and SWIR regions. Reflectance at 1135 and 1314 nm had strong linear relationships with ΔLWC ($r=-0.88, -0.88, p<0.01$) whereas reflectance at 1697 and 1642 nm had relatively lower correlations with ΔLWC ($r=-0.44, -0.38, p<0.05$). Danson et al. (1992) also obtained a similar finding that the first derivative of the reflectance spectrum at wavelengths corresponding to the slopes on the edges of the water absorption bands was highly correlated with leaf water content and insensitive to differences in leaf structure. In this study, the optimal RVI has a stronger relationship with water than any single reflectance band between 400 to 2400 nm, where the maximum R^2 value was 0.85 for reflectance at 1339 nm.

For estimating the changes of pigment content, the optimal RVI provided a higher

predictive accuracy than the optimal NDVI (Table 3). The chlorophylls have strong absorption peaks in the red and blue regions of the spectrum. Since the blue peak overlaps with the absorption of carotenoids, it is not generally used for the estimation of chlorophyll content. Maximum absorption in the red region occurs between 660 and 680 nm (Sims & Gamon, 2002). However, reflectance at these wavelengths has not proved as useful for predicting chlorophyll content as reflectance at slightly longer or shorter wavelengths. This is because, relatively low chlorophyll contents are sufficient to saturate absorption in the 660–680 nm region. Blackburn (1998) noted that reflectance along the wings of pigment absorption features are optimal in this context as they do not reach saturation but remain sensitive through a range of pigment concentrations and are not convoluted by other pigments. Estimation of leaf carotenoid content from reflectance is much more difficult than estimation of chlorophyll because of the overlap between the chlorophyll and carotenoid absorption peaks and the higher concentration of chlorophyll than carotenoid in most leaves. However, there was a higher predictive accuracy for ΔCars (RRMSEcv=0.3305) in our study compared to ΔChla, ΔChlb (RRMSEcv=0.6724, 1.4087). This is because the coefficient of determination between time and ΔCars is 0.49 during the post-thawing while the R^2 values of ΔChla (0.40), ΔChlb (0.18) during the post-thawing were relative lower. The optimal wavelength obtained by empirical methods such as regression can be affected by various factors including species, unit and range of pigment concentrations, data acquisition and preprocessing methods, and this may account for some of the disparities between the results presented in different papers. Overall, the results in this study indicate that vegetation indices have the potential to

571 estimate the changes in biochemical parameters that result from freezing injury.

572 Table 3. The optimal band positions for each type of spectral vegetation index and cross-validation
573 results for the accuracy of derived estimates of biochemical contents from the optimal indices.

VIs	Band position and R^2 values			Cross-validated statistics		
	R^2	λ1	λ2	R^2cv	RMSEcv (mg/cm^2)	RRMSEcv
ΔLWC						
NDVI	0.81	1135	1697	0.78	2.9400	0.2208
RVI	0.87	1314	1642	0.85	2.4161	0.1814
ΔChla						
NDVI	0.64	553	636	0.58	0.0044	0.7289
RVI	0.68	641	1295	0.65	0.0041	0.6724
ΔChlb						
NDVI	0.56	2110	2286	0.46	0.0013	1.5368
RVI	0.57	696	2155	0.53	0.0012	1.4087
ΔCars						
NDVI	0.65	648	676	0.61	0.0018	0.3791
RVI	0.73	641	959	0.70	0.0015	0.3305

574 **3.5.2 Quantification of biochemicals using multivariate statistical models**

575 **3.5.2.1 Changes in leaf water content**

576 The predictive accuracy of models for deriving ΔLWC from leaf reflectance spectra
577 using different multivariate techniques is summarized in Table 4. PLSR and PCR

performed better than SVMs for the first four spectral domains while the three techniques had similar estimation accuracies in the 1991-2400 nm regions. Although PLSR has an advantage over PCR in theory, in most situations, the methods achieve similar prediction accuracies and PCR usually needs more latent variables than PLSR (Mevik & Wehrens, 2007). The quality of SVMs models depends on the selection of kernel functions and the proper setting of hyper-parameters and kernel parameters. Whereas existing sources on SVMs regressions (Smola et al., 1998; Vapnik, 1998) give some recommendations on appropriate settings of SVMs parameters, there is no general consensus and there are many contradictory opinions. In this study, we used the most widely used grid search method to optimize the parameters by artificially specifying the parameters range. Some advanced intelligent optimization algorithms may improve the performance of SVMs such as the genetic algorithm, particle swarm optimization and the simulated annealing algorithm, and these approaches may be worthy of future investigation in the context of this research problem.

Amongst the five specific spectral domains tested, the best predictive accuracy for ΔLWC was achieved by using the full spectrum (with atmospheric water absorption bands removed) using PLSR and PCR, which produced the same R^2cv value of 0.85 and the same RMSEcv of 2.4408 (Table 4). The predicted accuracy of ΔLWC using only the 751-1349 nm spectral domain in PLSR and PCR was second to the full spectrum with R^2cv and RMSEcv values of 0.81 and 2.7272, respectively. The SWIR wavelength intervals 1481-1779 nm and 1991-2400 nm were superior to the visible region but inferior to the NIR region. The reason for this was that the strong water absorption bands

were removed from spectra before analysis in this study. From the perspective of multivariate statistical analysis, the full spectrum domain was optimal for retrieving water content. The optimal sub-spectral region needs further exploration, in order to improve the computational efficiency.

Table 4. Cross-validation statistics for predictive models in deriving ΔLWC from leaf spectral reflectance using three multivariate analysis techniques and three different spectral domains.

Spectral domains	Method	R^2cv	RMSEcv (mg/cm^2)	RRMSEcv
400-2400 nm	PLSR	0.85	2.4408	0.1833
	PCR	0.85	2.4408	0.1833
	SVMs	0.72	3.3699	0.2531
400-750 nm	PLSR	6.0E-04	6.5594	0.4926
	PCR	4.7E-02	6.4424	0.4838
	SVMs	3.5E-05	7.6421	0.5739
751-1349 nm	PLSR	0.81	2.7272	0.2048
	PCR	0.81	2.7272	0.2048
	SVMs	0.72	3.6441	0.2737
1481-1779 nm	PLSR	0.74	3.2321	0.2427
	PCR	0.69	3.5293	0.2651
	SVMs	0.62	3.9674	0.2979
1991-2400 nm	PLSR	0.54	4.3279	0.3250
	PCR	0.56	4.2605	0.3200
	SVMs	0.55	4.3614	0.3275

606 **3.5.2.2 Changes in the concentrations of leaf pigments**

607 The predictive accuracy of models for deriving ΔChla, ΔChlb and ΔCars from leaf
608 reflectance spectra using different multivariate techniques is summarized in Table 5. For
609 both spectral domains that were tested, PLSR and PCR had similarly high predictive
610 accuracies for ΔChla and ΔChlb. For ΔCars, PLSR and PCR exhibited similar predictive
611 accuracies when applied to the 400-900 nm domain, whereas for the 400-2400 nm domain,
612 PLSR had a higher predictive accuracy than that of PCR. When comparing the predictive
613 ability of the SVMs to the aforementioned methods, it can be observed that the PLSR
614 method produced superior predictive accuracies over SVMs for all leaf pigments for both
615 spectral domains. SVMs only achieved superiority over the PCR method in the estimation
616 of ΔCars when applied to the 400-900 nm spectral domain. Different methods displayed
617 different levels of effectiveness in the estimation of different biochemical parameters
618 which may be due to variations in the applicability of each algorithm. Similar to the
619 vegetation index results, the estimation accuracies for ΔChlb were poor for all three
620 methods and two spectral domains. This is likely due to the changes in Chlb during
621 post-thawing being minimal ($R^2 = 0.18$).

622 The estimation accuracy of each technique in the spectral domain 400-900 nm
623 outperformed the full spectrum for the prediction of all three pigments. Although this
624 optimal domain was only proposed for chlorophylls in the study of Huang & Blackburn
625 (2011), this domain is still optimal for all the individual pigments in our study using the
626 three multivariate regression techniques. This confirms that the 400-900 nm region is
627 most informative for the estimation of leaf pigment content.

628 Table 5. Cross-validation statistics in deriving ΔChla, ΔChlb and ΔCars from leaf spectral reflectance
629 using three multivariate analysis techniques and two different spectral domains.

Variable	Method	Spectral domains					
		400-2400 nm			400-900 nm		
		R^2cv	RMSEcv (mg/cm^2)	RRMSEcv	R^2cv	RMSEcv (mg/cm^2)	RRMSEcv
ΔChla	PLSR	0.29	0.0060	0.9836	0.36	0.0056	0.9254
	PCR	0.30	0.0062	1.0171	0.36	0.0056	0.9254
	SVMs	0.09	0.0070	1.1560	0.33	0.0058	0.9452
ΔChlb	PLSR	0.05	0.0019	2.1668	0.06	0.0018	2.0599
	PCR	0.05	0.0019	2.1668	0.06	0.0018	2.0599
	SVMs	0.06	0.0021	2.4141	0.01	0.0020	2.2723
ΔCar	PLSR	0.41	0.0023	0.4883	0.46	0.0021	0.4508
	PCR	0.21	0.0031	0.6638	0.46	0.0021	0.4508
	SVMs	0.38	0.0023	0.4824	0.47	0.0021	0.4450

630 **4. Conclusions**

631 In this study, we analyzed the changes in the spectral reflectance of oilseed rape
632 leaves that were subjected to freezing and post-thawing processes. We explored the
633 potential for using changes in spectral reflectance to detect the different stages of the
634 freezing and post-thawing processes, and to quantify the biochemical impacts of freezing
635 injury. The main findings are summarized as follows:

636 (1) The reflectance of leaves shows a significant decrease during freezing and then

637 remains constant across the optical spectrum as the freezing period continues. The
638 most significant spectral characteristic is that water absorption features shift towards
639 longer wavelengths, which is caused by the change of state of leaf water from liquid
640 to solid.
641 (2) In the process of post-thawing, the changes in spectral reflectance of leaves can
642 mainly be attributed to the changing water content of the leaf and the subsequent
643 changes in pigment content and cellular structure.
644 (3) SDR spectra exhibited the highest potential for discriminating leaves at different
645 stages of post-thawing from normal leaves.
646 (4) Derivative spectral indices formulated using optimized narrow wavebands were
647 most effective in quantifying the changes in pigment and water contents of leaves
648 subjected to freezing injury.
649 (5) In freezing injured leaves, the spectral domain 400-900 nm is optimal for
650 developing predictive models of pigment contents. Therefore, selection of this
651 spectral domain for analysis could reduce redundancy and increase computational
652 efficiency in future operational remote sensing scenarios.
653 This study focused on oilseed rape at the leaf scale in a laboratory setting. The results
654 provide evidence to establish the use of spectral reflectance for identifying different
655 stages of freezing injury in crops and quantifying the biochemical impacts of the process.
656 Further work is now needed to develop this capability by investigating freezing injury in
657 other crop species at the canopy and field scales using airborne and spaceborne
658 hyperspectral remotely-sensed data. Such developments have a considerable potential to

improve the monitoring and loss evaluation of freezing injury in crops when remotely sensed data of sufficiently high spatial, temporal and spectral resolution are available.

Acknowledgements

This study was supported by the National Natural Science Foundation of China (41171276) and the special fund for industrial and scientific research in the public interest (Meteorology) (GYHY201406028). The authors appreciate the valuable comments from anonymous reviewers.

References

Adjorlolo, C., Mutanga, O., & Cho, M.A. (2015). Predicting C3 and C4 grass nutrient variability using in situ canopy reflectance and partial least squares regression. *International Journal of Remote Sensing, 36*, 1743-1761.

Bak, J., Kim, J.H., Liu, X., Chance, K., & Kim, J. (2013). Evaluation of ozone profile and tropospheric ozone retrievals from GEMS and OMI spectra. *Atmospheric Measurement Techniques, 6*, 239-249.

Behmann, J., Steinruecken, J., & Pluemer, L. (2014). Detection of early plant stress responses in hyperspectral images. *ISPRS Journal of Photogrammetry and Remote Sensing, 93*, 98-111.

Berger, M., Moreno, J., Johannessen, J.A., Levelt, P.F., & Hanssen, R.F. (2012). ESA's sentinel missions in support of earth system science. *Remote Sensing of Environment, 120*, 84-90.

Blackburn, G.A. (1998). Spectral indices for estimating photosynthetic pigment concentrations: A test using senescent tree leaves. *International Journal of Remote Sensing, 19*, 657-675.

Board, S.S. (2007). Earth science and applications from space: National imperatives for the next decade and beyond. Washington, DC: National Academies Press.

Boser, B.E., Guyon, I.M., & Vapnik, V.N. (1992). A training algorithm for optimal margin classifiers. Proceedings of the Fifth Annual Workshop on Computational LearningTheory, p.144-152, Pittsburgh, Pennsylvania, USA.

Brown, M.S., Pereira, E.S.B., & Finkle, B.J. (1974). Freezing of nonwoody plant tissues Ⅱ. Cell damage and fine-structure of freezing curves. *Plant physiology, 53*, 709-711.

Burke, M.J., Gusta, L.V., Quamme, H.A., Weiser, C.J., & Li, P.H. (1976). Freezing and injury in plants. *Annual Review of Plant Physiology and Plant Molecular Biology, 27*, 507-528.

Carter, G.A. (1991). Primary and secondary effects of water content on the spectral reflectance of leaves. *American Journal of Botany, 78*, 916-924.

Ceccato, P., Gobron, N., Flasse, S., Pinty, B., & Tarantola, S. (2002). Designing a spectral index to estimate vegetation water content from remote sensing data: Part 1 - theoretical approach. *Remote Sensing*

of Environment, 82, 188-197.

Chang, C.C., & Lin, C.J. (2011). Libsvm: A library for support vector machines. http://www.csie.ntu.edu.tw/~cjlin/libsvm/.

Clark, R.N., & Roush, T.L. (1984). Reflectance spectroscopy quantitative analysis techniques for remote sensing applications. *Journal of Geophysical Research, 89*, 6329-6340.

Cortes, C., & Vapnik, V. (1995). Support vector networks. *Machine Learning, 20*, 273-297.

Cromey, M.G., Wright, D.S.C., & Boddington, H.J. (1998). Effects of frost during grain filling on wheat yield and grain structure. *New Zealand Journal of Crop and Horticultural Science, 26*, 279-290.

Croser, J.S., Clarke, H.J., Siddique, K.H.M., & Khan, T.N. (2003). Low temperature stress: Implications for chickpea (cicer arietinum l.) improvement. *Critical Reviews in Plant Sciences, 22*, 185-219.

Curran, P.J. (1989). Remote sensing of foliar chemistry. *Remote Sensing of Environment, 30*, 271-278.

Danson, F.M., Steven, M.D., Malthus, T.J., & Clark, J.A. (1992). High-spectral resolution data for determining leaf water content. *International Journal of Remote Sensing, 13*, 461-470.

Darvishzadeh, R., Skidmore, A., Schlerf, M., & Atzberger, C. (2008). Inversion of a radiative transfer model for estimating vegetation LAI and chlorophyll in a heterogeneous grassland. *Remote Sensing of Environment, 112*, 2592-2604.

Foody, G.M. (2002). Status of land cover classification accuracy assessment. *Remote Sensing of Environment, 80*, 185-201.

Foody, G.M., & Mathur, A. (2004). A relative evaluation of multiclass image classification by support vector machines. *IEEE Transactions on Geoscience and Remote Sensing, 42*, 1335-1343.

Galvao, L.S., dos Santos, J.R., Roberts, D.A., Breunig, F.M., Toomey, M., & de Moura, Y.M. (2011). On intra-annual EVI variability in the dry season of tropical forest: A case study with MODIS and hyperspectral data. *Remote Sensing of Environment, 115*, 2350-2359.

Gamon, J.A., Field, C.B., Bilger, W., Bjorkman, O., Fredeen, A.L., & Penuelas, J. (1990). Remote sensing of the xanthophyll cycle and chlorophyll fluorecence in sunflower leaves and canopies. *Oecologia, 85*, 1-7.

Gamon, J.A., & Surfus, J.S. (1999). Assessing leaf pigment content and activity with a reflectometer. *New Phytologist, 143*, 105-117.

Gao, L., Li, J., Khodadadzadeh, M., Plaza, A., Zhang, B., He, Z., & Yan, H. (2015). Subspace-based support vector machines for hyperspectral image classification. *IEEE Geoscience and Remote Sensing Letters, 12*, 349-353.

Gausman, H.W., Burke, J.J., & Quisenberry, J.E. (1984). Use of leaf optical properties in plant stress research. *ACS Symposium Series, 257*, 215-233.

Gleason, C.J., & Im, J. (2012). Forest biomass estimation from airborne LiDAR data using machine learning approaches. *Remote Sensing of Environment, 125*, 80-91.

Gonzalez-Fernandez, A.B., Rodriguez-Perez, J.R., Marabel, M., & Alvarez-Taboada, F. (2015). Spectroscopic estimation of leaf water content in commercial vineyards using continuum removal and partial least squares regression. *Scientia Horticulturae, 188*, 15-22.

Gowen, A.A., Taghizadeh, M., & O'Donnell, C.P. (2009). Identification of mushrooms subjected to freeze damage using hyperspectral imaging. *Journal of Food Engineering, 93*, 7-12.

Green, R.O., Painter, T.H., Roberts, D.A., & Dozier, J. (2006). Measuring the expressed abundance of the three phases of water with an imaging spectrometer over melting snow. *Water Resources Research, 42*.

Guy, C.L. (1990). Cold acclimation and freezing stress tolerance: Role of protein metabolism. *Annual Review of Plant Physiology and Plant Molecular Biology, 41*, 187-223.

Hichri, H., Bazi, Y., Alajlan, N., & Malek, S. (2013). Interactive segmentation for change detection in multispectral remote sensing images. *IEEE Geoscience and Remote Sensing Letters, 10*, 298-302.

Hong, G., Wang, S., Li, J., & Huang, J. (2015). Fully polarimetric synthetic aperture radar (SAR) processing for crop type identification. *Photogrammetric Engineering & Remote Sensing, 81*, 109-117.

Huang, J.F., & Blackburn, G.A. (2011). Optimizing predictive models for leaf chlorophyll concentration based on continuous wavelet analysis of hyperspectral data. *International Journal of Remote Sensing, 32*, 9375-9396.

Hussain, M., Chen, D., Cheng, A., Wei, H., & Stanley, D. (2013). Change detection from remotely sensed images: From pixel-based to object-based approaches. *ISPRS Journal of Photogrammetry and Remote Sensing, 80*, 91-106.

Inoue, Y., Sakaiya, E., Zhu, Y., & Takahashi, W. (2012). Diagnostic mapping of canopy nitrogen content in rice based on hyperspectral measurements. *Remote Sensing of Environment, 126*, 210-221.

Jensen, J.R. (2006). Remote sensing of the environment: An earth resource perspective. (2nd Edition ed.). New Jersey: Prentice Hall, (Chapter 11).

Jordan, C.F. (1969). Derivation of leaf area index from quality of light on forest floor. *Ecology, 50*, 663-666.

Knipling, E.B. (1970). Physical and physiological basis for the reflectance of visible and near-infrared radiation from vegetation. *Remote Sensing of Environment*, 155-159.

Kooistra, L., Salas, E.A., Clevers, J.G., Wehrens, R., Leuven, R.S., Nienhuis, P.H., et al. (2004). Exploring field vegetation reflectance as an indicator of soil contamination in river floodplains. *Environmental Pollution, 127*, 281-290.

Lardon, A., & TriboiBlondel, A.M. (1995). Cold and freeze stress at flowering: Effects on seed yields in winter rapeseed. *Field Crops Research, 44*, 95-101.

Lichtenthaler, H.K. (1987). Chlorophylls and carotenoids: Pigments of photosynthetic biomembranes. *Methods in Enzymology, 148*, 350-382.

Liu, Z., Huang, F., Li, L., & Wan, E. (2002). Dynamic monitoring and damage evaluation of flood in north-west jilin with remote sensing. *International Journal of Remote Sensing, 23*, 3669-3679.

Mantero, P., Moser, G., & Serpico, S.B. (2005). Partially supervised classification of remote sensing images through SVM-based probability density estimation. *IEEE Transactions on Geoscience and Remote Sensing, 43*, 559-570.

Mevik, B.H., & Wehrens, R. (2007). The pls package: Principal component and partial least squares regression in R. *Journal of Statistical Software, 18*, 1-23.

Mirzaie, M., Darvishzadeh, R., Shakiba, A., Matkan, A.A., Atzberger, C., & Skidmore, A. (2014). Comparative analysis of different uni- and multi-variate methods for estimation of vegetation water content using hyper-spectral measurements. *International Journal of Applied Earth Observation and Geoinformation, 26*, 1-11.

Nemmour, H., & Chibani, Y. (2006). Multiple support vector machines for land cover change detection: An application for mapping urban extensions. *ISPRS Journal of Photogrammetry and Remote Sensing, 61*, 125-133.

Nicotra, A.B., Hofmann, M., Siebke, K., & Ball, M.C. (2003). Spatial patterning of pigmentation in evergreen leaves in response to freezing stress. *Plant Cell and Environment, 26*, 1893-1904.

Penuelas, J., Filella, I., Biel, C., Serrano, L., & Save, R. (1993). The refectance at the 950-970 nm region as an indicator of plant water status. *International Journal of Remote Sensing, 14*, 1887-1905.

Price, J.C. (1994). How unique are spectral signatures?. *Remote Sensing of Environment, 49*, 181-186.

Richardson, A.D., Duigan, S.P., & Berlyn, G.P. (2002). An evaluation of noninvasive methods to estimate foliar chlorophyll content. *New Phytologist, 153*, 185-194.

Rouse, J.W., Haas, R.H., & Schell, J.A. (1974). Monitoring vegetation systems in the great plains with ERTS, NASA SP-351. Third ERTS-1 Symposium, Vol. 1, pp. 309–317, NASA, Washington, DC.

Sankaran, S., Mishra, A., Ehsani, R., & Davis, C. (2010). A review of advanced techniques for detecting plant diseases. *Computers and Electronics in Agriculture, 72*, 1-13.

Savitzky, A., & Golay, M.J.E. (1964). Smoothing and differentiation of data by simplified least squares procedures. *Analytical Chemistry, 36*, 1627-1639.

She, B., Huang, J.f., Guo, R.f., Wang, H.b., & Wang, J. (2015). Assessing winter oilseed rape freeze injury based on Chinese HJ remote sensing data. *Journal of Zhejiang University Science B, 16*, 131-144.

Sims, D.A., & Gamon, J.A. (2002). Relationships between leaf pigment content and spectral reflectance across a wide range of species, leaf structures and developmental stages. *Remote Sensing of Environment, 81*, 337-354.

Slaton, M.R., Hunt, E.R., & Smith, W.K. (2001). Estimating near-infrared leaf reflectance from leaf structural characteristics. *American Journal of Botany, 88*, 278-284.

Smola, A.J., Murata, N., Schölkopf, B., & Müller, K.R. (1998). Asymptotically optimal choice of ε-loss for support vector machines. Proceedings of the International Conference on Artificial Neural Networks, (pp. 105−110). Berlin: Springer. http://citeseer.ist.psu.edu/26614.html.

Staggenborg, S.A., & Vanderlip, R.L. (1996). Sorghum grain yield reductions caused by duration and timing of freezing temperatures. *Agronomy Journal, 88*, 473-477.

Strachan, I.B., Pattey, E., & Boisvert, J.B. (2002). Impact of nitrogen and environmental conditions on corn as detected by hyperspectral reflectance. *Remote Sensing of Environment, 80*, 213-224.

Team, R.C. (2014). R: A language and environment for statistical computing. R Foundation for Statistical Computing: Vienna, Austria.

Thenkabail, P.S., Smith, R.B., & Pauw, E.D. (2000). Hyperspectral vegetation indices and their relationships with agricultural crop characteristics. *Remote Sensing of Environment, 71*, 158-182.

Thyholt, K., & Isaksson, T. (1997). Differentiation of frozen and unfrozen beef using near-infrared spectroscopy. *Journal of the Science of Food and Agriculture, 73*, 525-532.

Tsai, F., & Philpot, W. (1998). Derivative analysis of hyperspectral data. *Remote Sensing of Environment, 66*, 41-51.

Vapnik, V.N. (1998). Statistical learning theory. New York: Wiley-Interscience.

Verrelst, J., Munoz, J., Alonso, L., Delegido, J., Pablo Rivera, J., Camps-Valls, G., et al. (2012). Machine learning regression algorithms for biophysical parameter retrieval: Opportunities for Sentinel-2 and -3. *Remote Sensing of Environment, 118*, 127-139.

Wang, H.f., Huo, Z.g., Zhou, G.s., Liao, Q.h., Feng, H.k., & Wu, L. (2016). Estimating leaf spad values of freeze-damaged winter wheat using continuous wavelet analysis. *Plant Physiology and Biochemistry, 98*, 39-45.

Wang, H.F., Wang, J.H., Wang, Q., Miao, N.Z., Huang, W.J., Feng, H.K., et al. (2012). Hyperspectral characteristics of winter wheat under freezing injury stress and LWC inversion model. First international conference on agro-geoinformatics. pp. 141-146, Shanghai, China.

Xin, Z., & Browse, J. (2000). Cold comfort farm: The acclimation of plants to freezing temperatures. *Plant Cell and Environment, 23*, 893-902.

Yang, X., Huang, J., Wu, Y., Wang, J., Wang, P., Wang, X., et al. (2011). Estimating biophysical parameters of rice with remote sensing data using support vector machines. *Science China Life Sciences, 54*,

272-281.

Ye, X., Sakai, K., Sasao, A., & Asada, S.i. (2008). Potential of airborne hyperspectral imagery to estimate fruit yield in citrus. *Chemometrics and Intelligent Laboratory Systems, 90*, 132-144.

Yi, Q.X., Bao, A.M., Wang, Q., & Zhao, J. (2013). Estimation of leaf water content in cotton by means of hyperspectral indices. *Computers and Electronics in Agriculture, 90*, 144-151.

Yu, K., Lenz-Wiedemann, V., Chen, X., & Bareth, G. (2014). Estimating leaf chlorophyll of barley at different growth stages using spectral indices to reduce soil background and canopy structure effects. *ISPRS Journal of Photogrammetry and Remote Sensing, 97*, 58-77.

Zhai, Y.F., Cui, L.J., Zhou, X., Gao, Y., Fei, T., & Gao, W.X. (2013). Estimation of nitrogen, phosphorus, and potassium contents in the leaves of different plants using laboratory-based visible and near-infrared reflectance spectroscopy: Comparison of partial least square regression and support vector machine regression methods. *International Journal of Remote Sensing, 34*, 2502-2518.

Zhang, C., Wang, T., Atkinson, P.M., Pan, X., & Li, H. (2015). A novel multi-parameter support vector machine for image classification. *International Journal of Remote Sensing, 36*, 1890-1906.

Zhang, X., Zhang, C., Liao, X., & Wang, H. (2008). Investigation on 2008 low temperature and freeze injury on winter rape along Yangtze river. *Chinese Journal of Oil Crop Sciences, 30*, 122-126.

List of Figure Captions

Fig. 1. Minimum and maximum daily temperatures in Hangzhou, China; (a) between October 2013 and December 2013, and (b) between October 2014 and February 2015. The treatment dates are indicated by gray vertical bars. Closed and open circles represent maximum and minimum temperature, respectively.

Fig. 2. Changes of leaf temperature during freezing treatment.

Fig. 3. Average SPAD values of oilseed rape leaves at the normal, supercooling, 1hr of freezing and at different hours of post-thawing. The bars represent ± 95% confidence interval (CI) (n=26).

Fig. 4. Light microscopic images (a, b) and transmission electron micrographs (c, d) showing transverse section of normal (a, c) and freeze-damaged (b, d) oilseed rape leaves.

Fig.5. Response of leaf reflectance spectra at different phases of freezing injury: (a) changes in average reflectance with freezing; (b) changes in average reflectance with

855 post-thawing. N, F and PT represent normal, freezing and post-thawing in the Legend.
856 The total sample sizes are 5 and 26, respectively.

857 Fig. 6. Change in indices θ and D; (a-f) during freezing, and (g-l) post-thawing. N
858 represents normal state, F-digit denotes the duration of freezing, PT-digit means the time
859 of post-thawing. Bars represent 95% confidence interval.

860